Urease-Coated Polydopamine Nanomotors as Self-Propelled Biosensors for Non-Invasive Diagnosis: Detection of Prostate Cancer-Associated miR-141 in Urine

Semanur Özcan Özseven[1], Gözde Yurdabak Karaca[2], Lütfi Öksüz[3,4], Joseph Wang[5], Ayşegül Uygun Öksüz[6*]

[1]Suleyman Demirel University, Graduate School of Natural and Applied Sciences, Bioengineering 32260 ISPARTA/TURKEY

[2]Suleyman Demirel University, Isparta Health Services Vocational School, Medical Services and Techniques, 32260 ISPARTA/TURKEY

[3]Suleyman Demirel University, Faculty of Engineering and Natural Sciences, Department of Physics, 32260 ISPARTA/TURKEY

[4]PLAZMATEK, Süleyman Demirel University Technokent, No: 105, 32000 ISPARTA/TURKEY

[5] [e]Aiiso Yufeng Li Family Department of Chemical and Nano Engineering, University of California San Diego, La Jolla, CA 92093, USA

[6]Suleyman Demirel University, Faculty of Engineering and Natural Sciences, Department of Chemistry, 32260 ISPARTA/TURKEY

Corresponding author: ayseguluygunoksuz@gmail.com

Figure Captions:

Figure S1. EDS spectrum / PDA analysis result

Figure S2. EDS spectrum / PDA/PLL analysis result

Figure S3. EDS spectrum / PDA/PLL@UR analysis result

Figure S4. Hydrodynamic size distribution of PDA, PDA/PLL, and PDA/PLL@UR nanomotors (DLS analysis)

Figure S5. FT-IR spectra of PDA, PDA/PLL, PDA/PLL@UR, and FAM-ssDNA-PDA/PLL@UR

Figure S5. The XPS O1s spectra

Figure S6. The XPS N1s spectra

Figure S7. XPS C1s spectrum

Figure S8. The P2p XPS spectrum shows a P–O peak

Figure S9. Decrease in fluorescence intensity (FI) observed with increasing miR-141 concentration

Figure S10. Fluorescence response to miR-141

Figure S11. Intraday and interday variation of nanomotor speed

Figure S12. Intraday and interday variation of fluorescence intensity

Figure S13: Tukey HSD results for nanomotor speed (a) and fluorescence quenching (b).

Figure S14: Interday statistical analysis of nanomotor speed and fluorescence intensity.

Table Captions:

Table S1: One-way ANOVA results for nanomotor speed and fluorescence intensity.

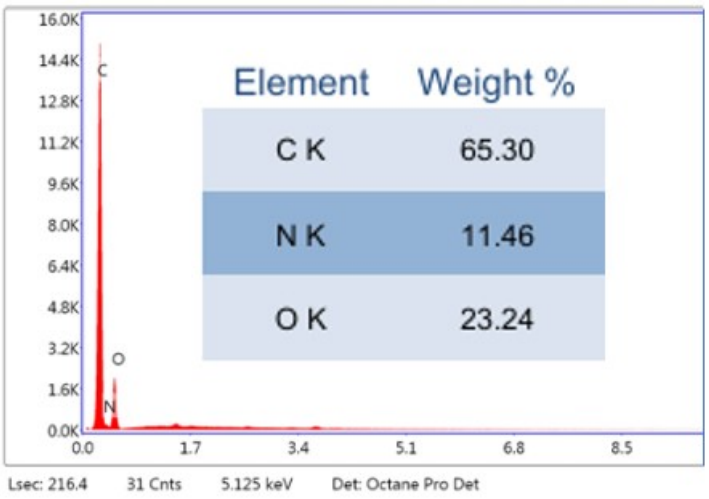

Figure S1. EDS spectrum / PDA analysis result

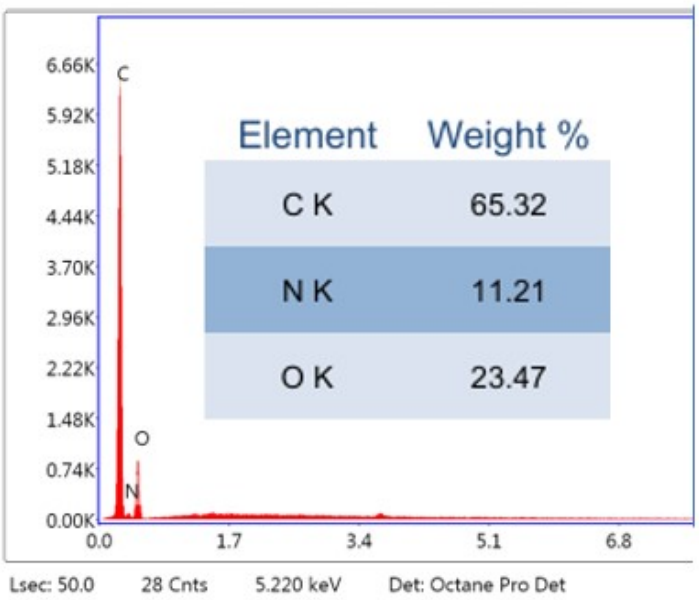

Figure S2: EDS spectrum / PDA/PLL analysis result

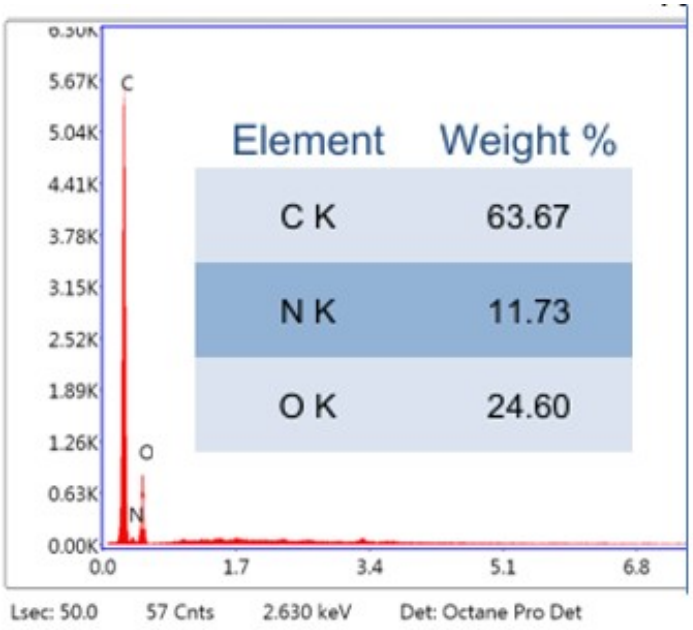

Figure S3: EDS spectrum / PDA/PLL@UR analysis result

Hydrodynamic Size Distribution of PDA, PDA/PLL, and PDA/PLL@UR Nanomotors

Hydrodynamic size distributions obtained by dynamic light scattering (DLS) are larger than the sizes observed in SEM due to fundamental differences between the two techniques. DLS measures the hydrodynamic diameter, which includes not only the particle core but also the surrounding solvation layer and any adsorbed molecules. In addition, DLS is highly sensitive to aggregation, as larger aggregates scatter light more intensely and can influence the measured size distribution (Mota et al., 2025).

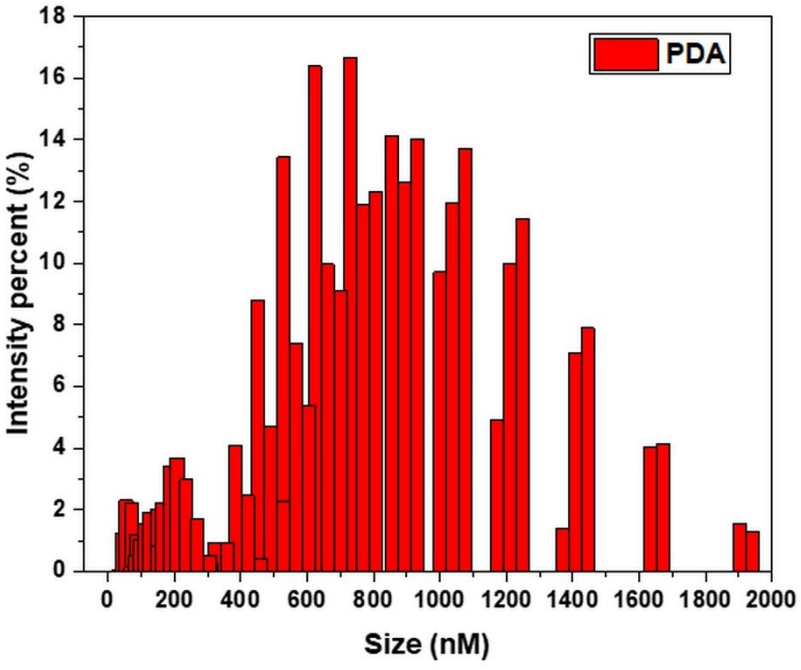

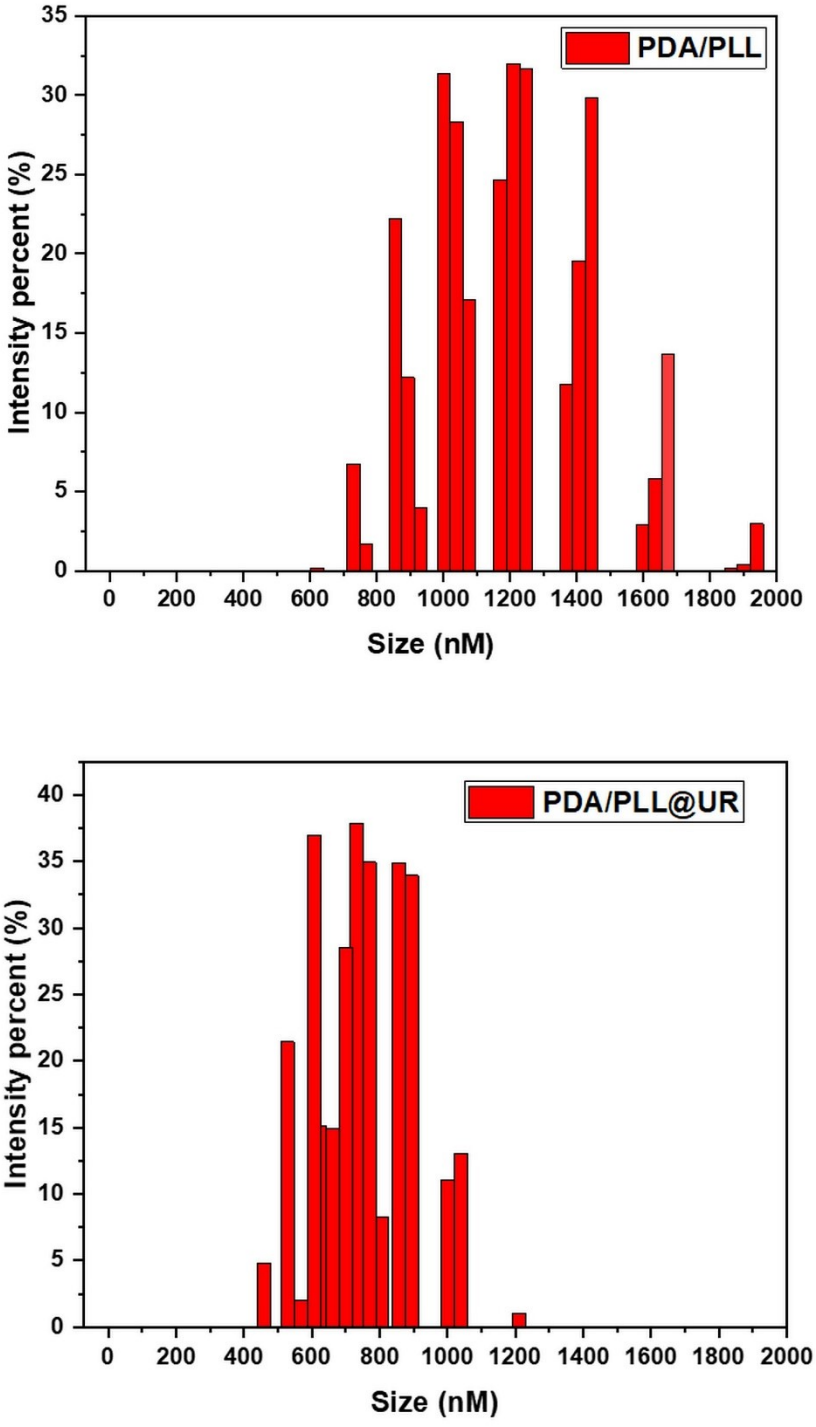

Figure S4: Hydrodynamic size distribution profiles of PDA, PDA/PLL, and PDA/PLL@UR nanomotors obtained by dynamic light scattering (DLS).

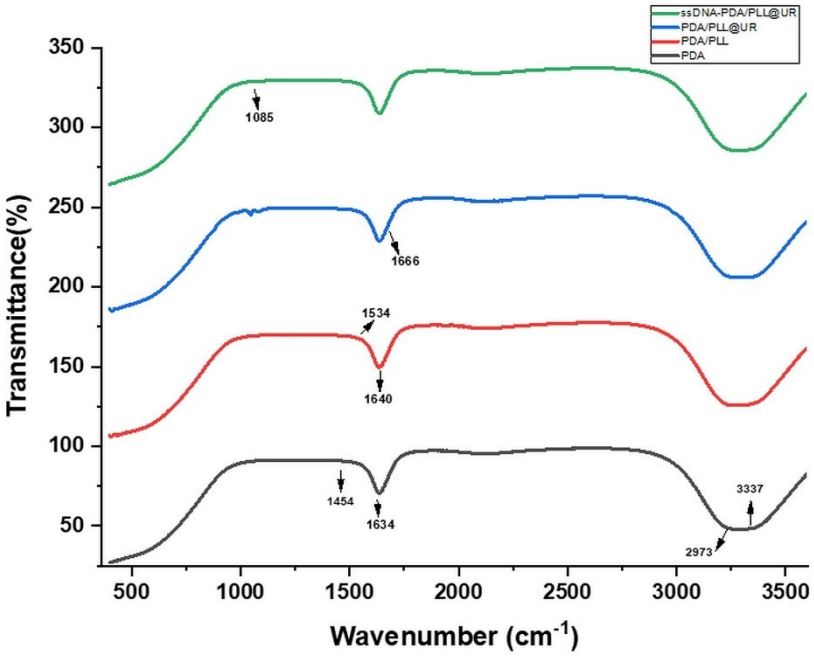

Figure S5: FT-IR spectra of PDA, PDA/PLL, PDA/PLL@UR, and FAM-ssDNA-PDA/PLL@UR

Comprehensive Zeta Potential Analysis Results of the Nanomotors

Phase–time, total counts–zeta potential and size (d.nm)–percent distributions profiles of the nanomotors (P1–P5). P1: PDA nanomotors, P2: PDA/PLL nanomotors, P3: PDA/PL@UR nanomotors and P4: FAM-ssDNA-PDA/PLL@UR nanomotors. These graphs demonstrate the phase stability and surface charge distribution of each nanomotor type. PDA, PDA/PLL, PDA/PLL@UR, FAM-ssDNA-PDA/PLL@UR nanomotors were coded as P1, P2, P3 and P4, respectively.

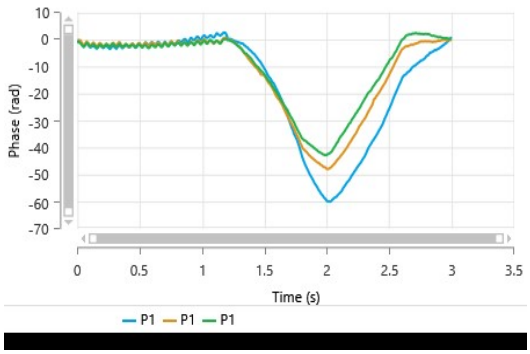

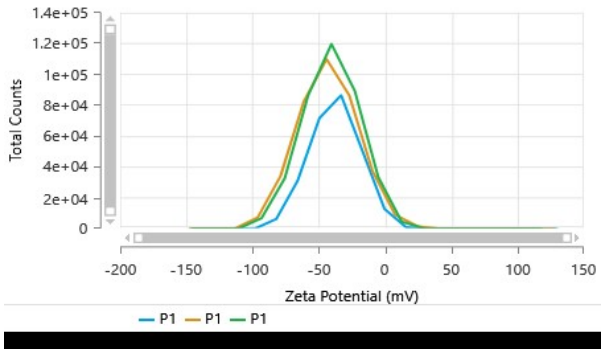

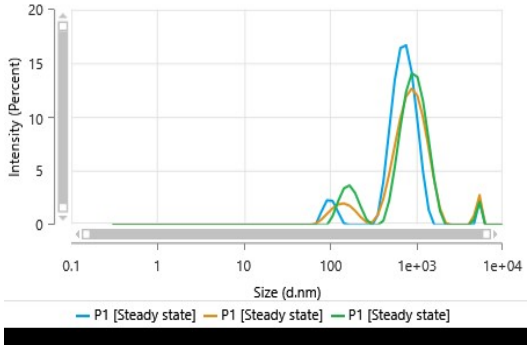
Intensity (Percent)
Size (d.nm)
P1 [Steady state] P1 [Steady state] P1 [Steady state]

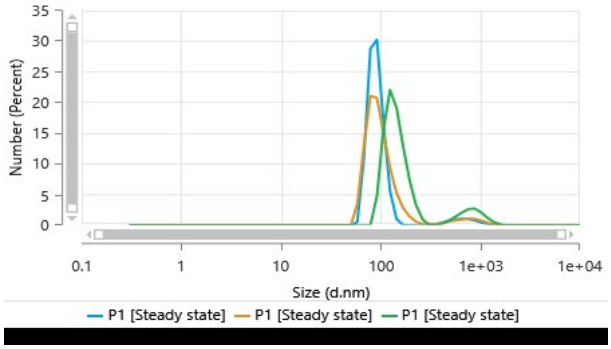
Number (Percent)
Size (d.nm)
P1 [Steady state] P1 [Steady state] P1 [Steady state]

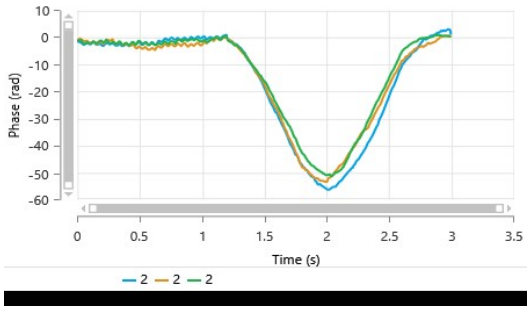
Phase (rad)
Time (s)
2 2 2

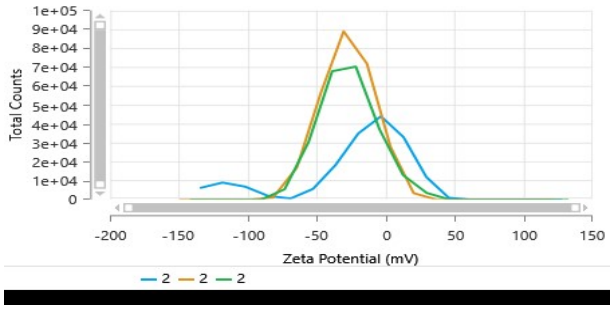
Total Counts
Zeta Potential (mV)
2 2 2

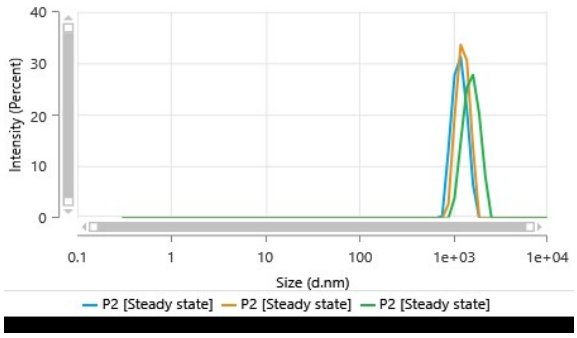
Intensity (Percent)
Size (d.nm)
P2 [Steady state] P2 [Steady state] P2 [Steady state]

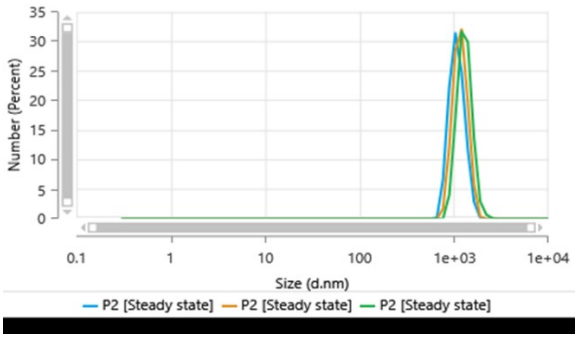
Number (Percent)
Size (d.nm)
P2 [Steady state] P2 [Steady state] P2 [Steady state]

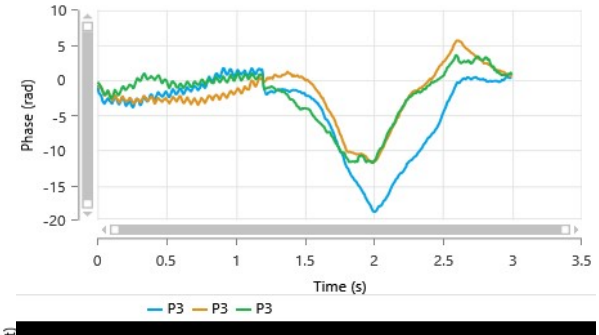
Phase (rad)
Time (s)
P3 P3 P3

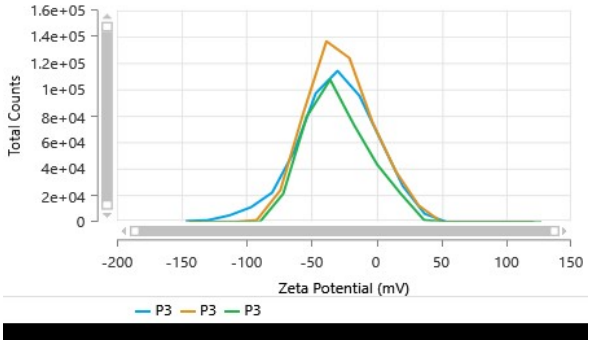
Total Counts
Zeta Potential (mV)
P3 P3 P3

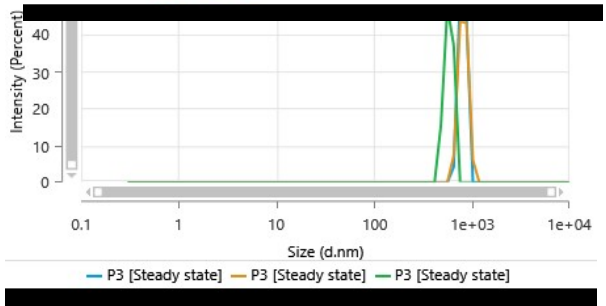
Intensity (Percent)
Size (d.nm)
P3 [Steady state] P3 [Steady state] P3 [Steady state]

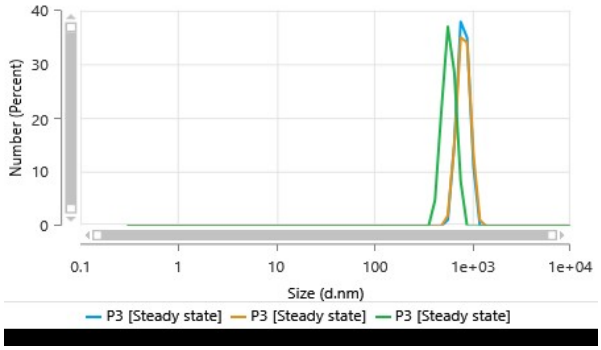

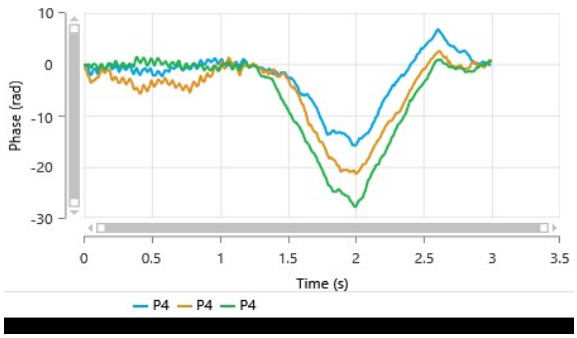

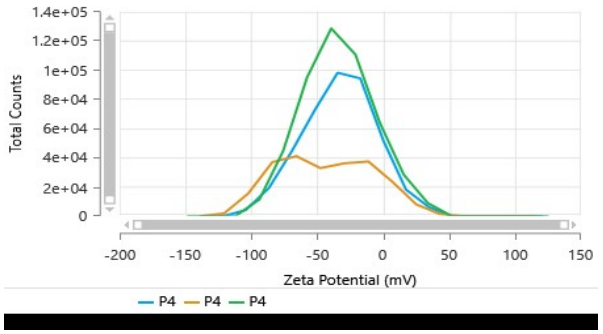

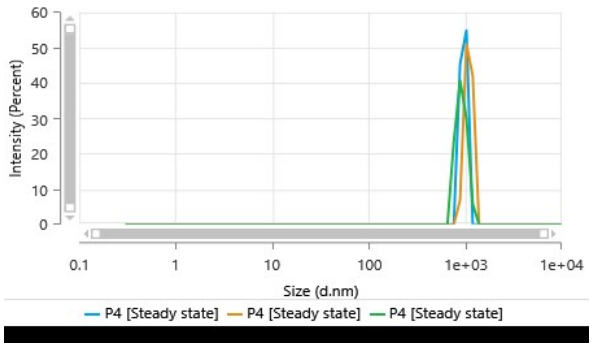

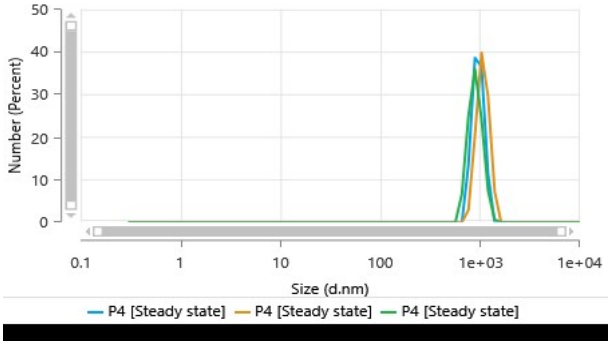

Figure S6: Hydrodynamic size distributions obtained by dynamic light scattering (DLS)

XPS spectra showing binding energy (e.V) and intensity (a.u) for the nanomotor samples. The

corresponding atomic percentages of O1s, N1s, C1s, and P-O were calculated from peak areas.

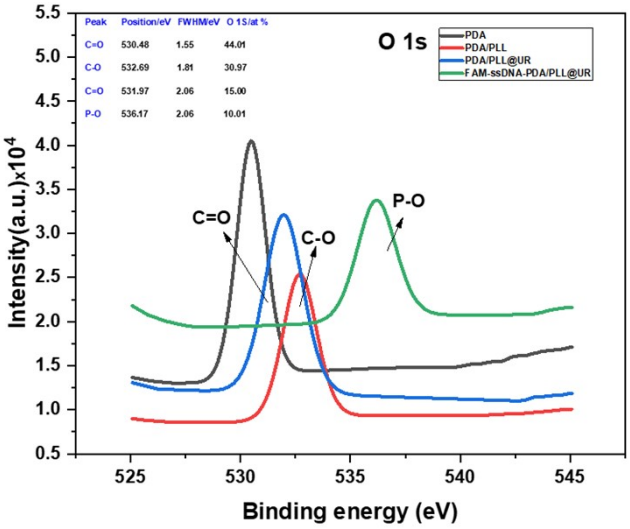

Figure S7: The XPS O1s spectra show dominant C=O and C–O groups on the PDA surface. Upon PLL binding, the C–O signals increase, and a distinct P–O peak appears after FAM-ssDNA immobilization. These changes confirm successful surface modification and functionalization of the nanomotors.

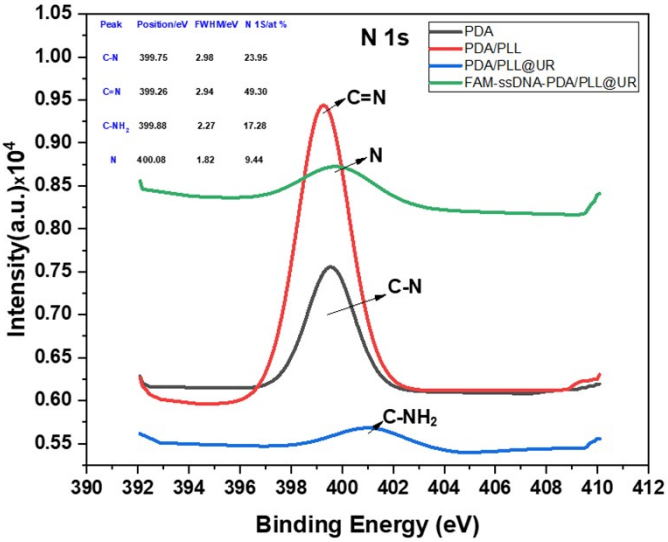

Figure S8: The XPS N1s spectra show that C–N groups are present on the PDA surface initially. Upon PLL binding, C=N signals become dominant, indicating that PLL attachment induces the formation of new C=N structures or modification of existing amine groups, confirming the functionalization of the nanomotor surface. The appearance of a new peak after FAM-ssDNA immobilization further verifies the successful binding of the target molecule.

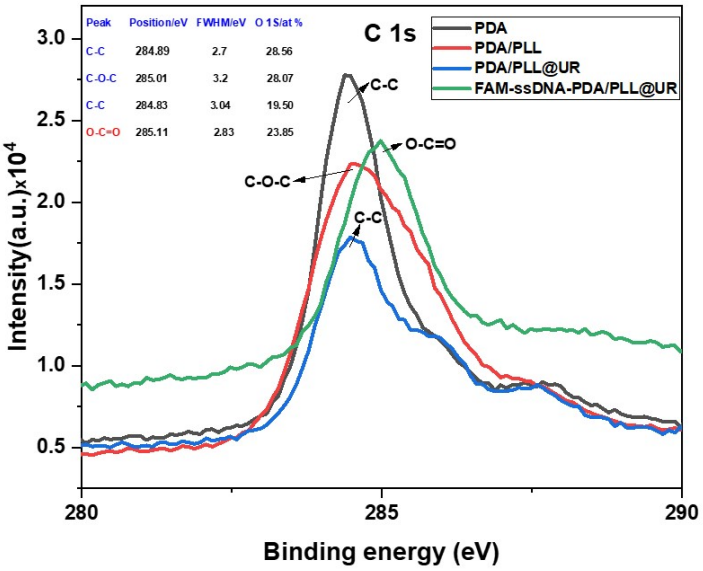

Figure S9: XPS C1s spectrum showing C–C (~284.6 eV) and C–O–C groups on the PDA surface. The peak shifts to ~286 eV, indicating an increase in O–C=O bonds contributed by FAM-ssDNA; this change confirms successful surface modification upon PLL binding or FAM-ssDNA immobilization.

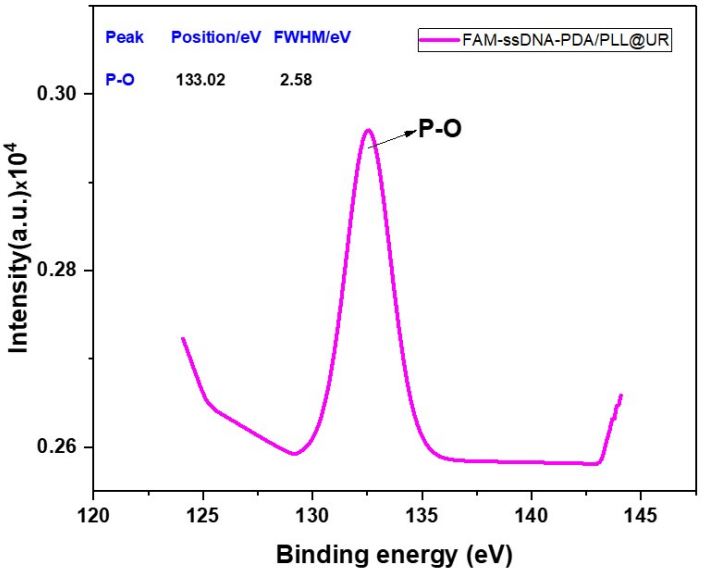

Figure S10: The P2p XPS spectrum shows a P–O peak.

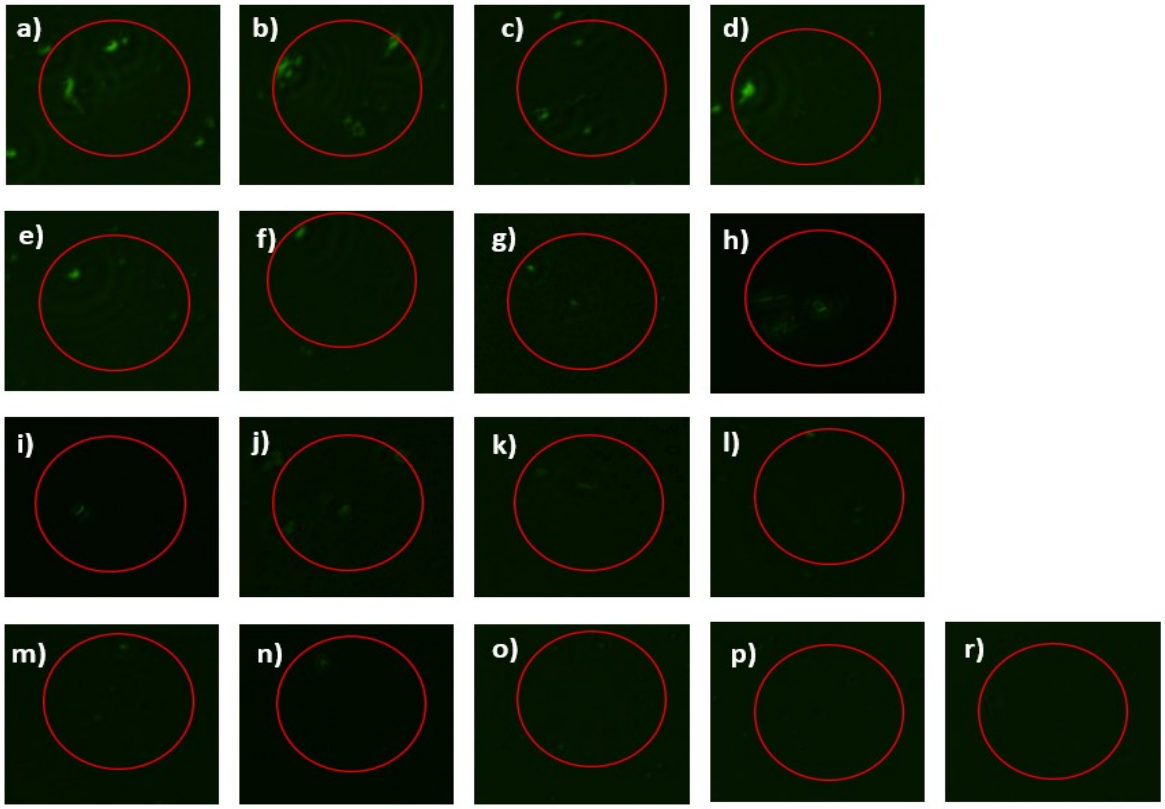

Figure S11. Decrease in fluorescence intensity (FI) observed with increasing miR-141 concentration **a)** PDA+ssDNA, **b)** 6,25x10^{-5}nM miR-141, **c)** 1,25x10^{-4}nM miR-141, **d)** 2,5x10^{-4}nM miR-141, **e)** 5x10^{-4}nM miR-141, **f)** 0.01 nM miR-141, **g)** 0.01 nM miR-141, **h)** 0.05 nM miR-141, **i)** 0.1 nM miR-141, **j)** 0,25 nM miR-141, **k)** 0,5 nM miR-141, **l)** 1 nM miR-141, **m)** 2,5 nM miR-141, **n)** 5 nM miR-141 **o)** 25 nM miR-141, **p)** 50 nM miR-141, **r)**100 nM miR-141

Precision, Reproducibility and Stability of the Biosensor

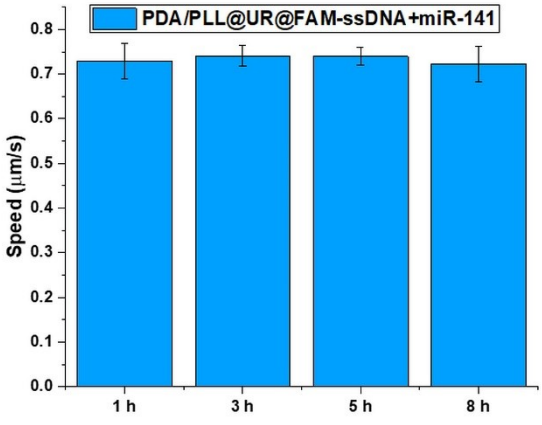

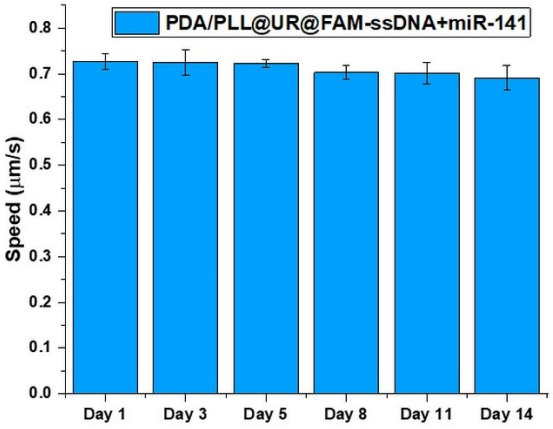

Figure S12: Intraday variations of nanomotor speed measured at 1, 3, 5, and 8 hours.

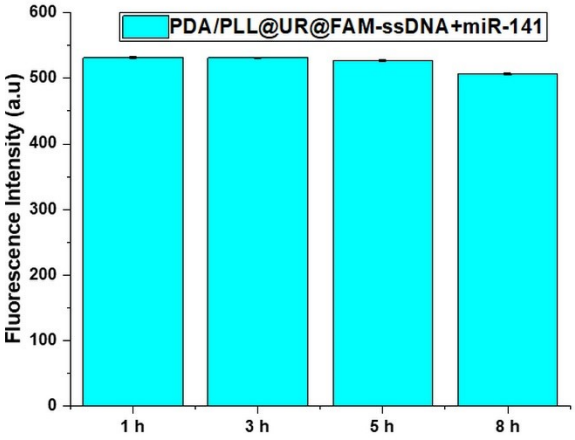

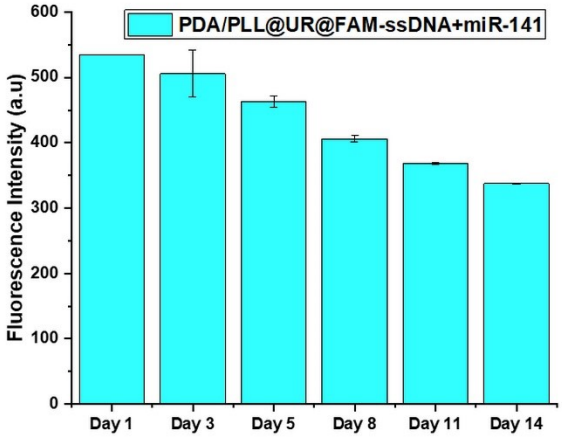

Figure S13: Interday variations of nanomotor fluorescence intensity measured on days 1, 3, 5, 8, 11, and 14.

Statistical Analysis

The effect of time on the speed of nanomotors synthesized and stored at +4 °C was evaluated based on the following hypotheses:

H_o: Time has no effect on the speed of nanomotors stored at +4 °C.
H_1: Time has an effect on the speed of nanomotors stored at +4 °C.

To test the hypothesis, nanomotor speed and fluorescence intensity were evaluated through 10 replicate measurements, both intraday (at 1, 3, 5, and 8 hours) and interday (on days 1, 3, 5, 8, 11, and 14). The obtained data were analyzed using one-way analysis of variance (one-way ANOVA), and Tukey's multiple comparison test was applied to determine differences between groups.

Tablo S1. One-way ANOVA results for intraday nanomotor speed and fluorescence intensity

		Sum of Squares	df	Mean Square	F	Sig.
Speed_1day	Between Groups	,002	3	,001	,515	**,675**
	Within Groups	,052	36	,001		
	Total	,054	39			
Fluor_1day	Between Groups	4076,900	3	1358,967	554,680	**,000**
	Within Groups	88,200	36	2,450		
	Total	4165,100	39			

Figure S14: Tukey HSD results for nanomotor speed (a) and fluorescence quenching (b).

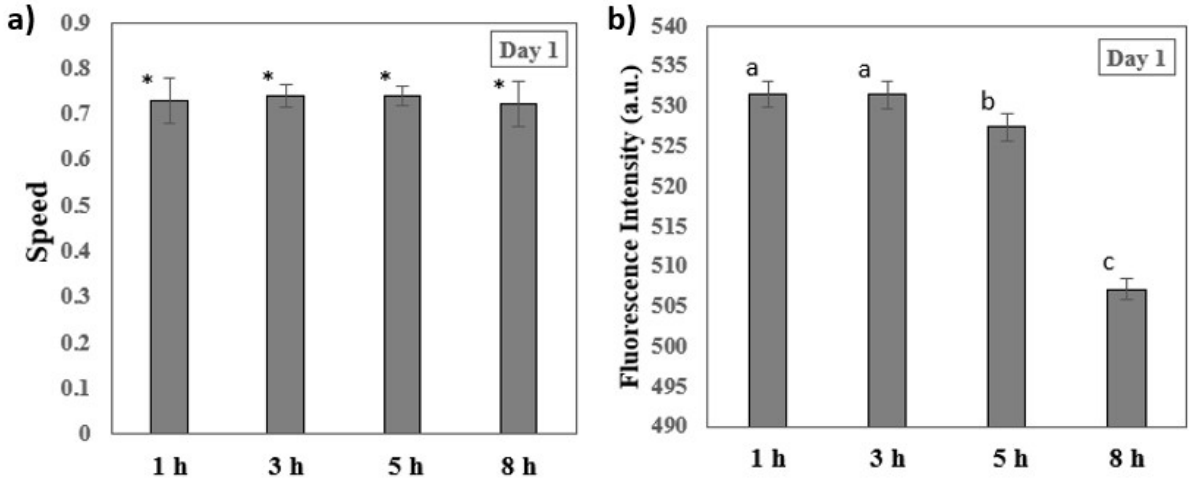

*There is no statistically significant difference between the groups.

a, b, c: Groups sharing the same letters are not significantly different.

Figure S15: Interday analysis showing stable nanomotor speed and significant fluorescence changes

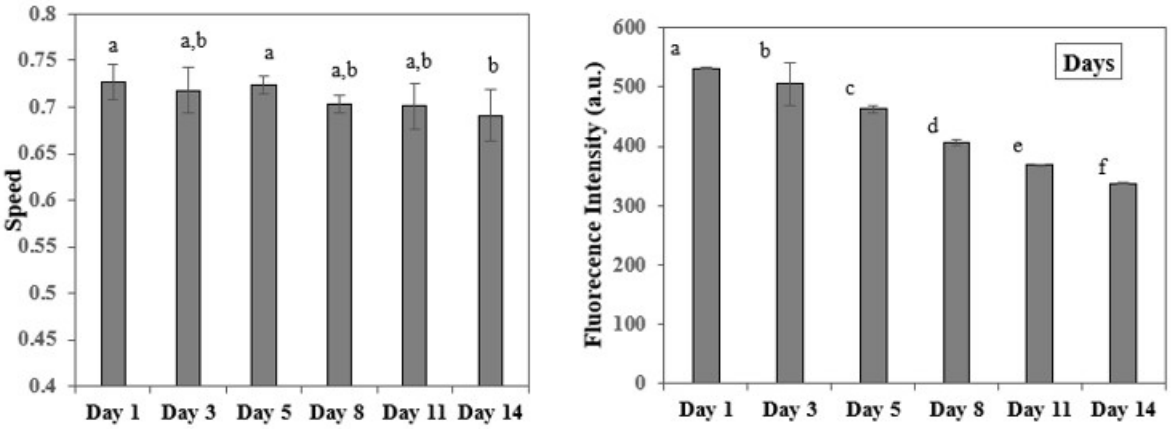

a,b There is a statistically significant difference between the

groups.

a–f: Groups with different letters indicate statistically significant differences.

References

Mota, W. S., Severino, P., Kadian, V., Rao, R., Zielińska, A., Silva, A. M., Mahant, S., & Souto, E. B. (2025). Nanometrology: particle sizing and influence on the toxicological profile. In *Frontiers in Nanotechnology* (Vol. 7).